International Journal of Networks and Communications 2019, 9(1): 37-52
DOI: 10.5923/j.ijnc.20190901.03

Performance Comparison between O- and C-bands Optical Carrier-Assisted Nyquist Half-Cycle SSB Communication Systems

Mays M. Ibrahim*, Raad S. Fyath

Department of Computer Engineering, Al-Nahrain University, Baghdad, Iraq

Abstract This paper investigates the noise characteristics and transmission performance of Nyquist half-cycle single-sideband system incorporating amplified or unamplified optical link. The system design is based on intensity modulation/optical carrier assisted direct detection scheme. Digital signal processing is used at the receiver to compensate dispersion and nonlinearity of the optical fiber. Simulation results are presented for both 1310 and 1550 nm single-channels carrying 224 Gbps 16-QAM data. The results are used as a guideline to extend the results for O- and C-band wavelength division multiplexing (WDM) systems. The maximum transmission distance L_{max} is deduced for different systems using a bit error rate threshold of 4.5×10^{-3} which corresponds to 7% overhead decision forward error correcting code. The results reveal that L_{max} of the unamplified 1550 nm single-channel system is about 1.75 time that of the 1310 nm counterpart. The simulation is reversed when optical amplifiers are used to compensate fiber loss leading to higher transmission distance at 1310 nm. Further, using 0 dB carrier and signal lasers offer 44 and 72 km transmission distance for the unamplified 16-channel WDMs operating at O- and C-bands, respectively. Inserting optical amplifiers changes these values to 450 and 110 km, respectively. The simulation results are performance using Optisystem ver. 14 and are in good agreement with published experimental data.

Keywords Nyquist half cycle (NHC) optical communication, O- and C-bands NHC, 16-QAM IM/DD, Optical SSB 16-QAM

1. Introduction

The emerging advanced optical networks face two main challenges related to the transmission capacity and user-end cost [1-5]. To deal with the increasing traffic demand associated with advanced data application based on internet of things (IOT) and cloud computing, the network should adopt advanced optical communication techniques [6-8]. Among these techniques are high-order modulation to increase the number of bits carried by the transmitting symbol [9, 10] and using multiplexing technique to transmit multichannel on the same link [3, 11, 12]. To reduce the cost at the user end, intensity modulation/direct detection (IM/DD) schemes are preferred to be used [13-15]. The DD receiver does not use a local laser source for the detection process and hence reduces the cost and increases the receiver robustness [16, 17]. Different IM/DD schemes have been used in optical networks such as orthogonal frequency-division multiplexing (OFDM) [18, 19], carrierless amplitude phase (CAP) modulation [5, 20], and subcarrier multiplexing (SCM) [21, 22]. The SCM scheme attracts increasing interest since it does not need high-speed numerical calculations when compared with OFDM, which uses fast Fourier transform, and CAP which uses virtual in-phase (I) and quadrature-phase (Q) filters.

To increase the spectral efficiency (SE) of the SCM scheme, the following points should be taken into the consideration

(i) Modulating the subcarrier by high-order modulation formats such as quadrature-amplitude modulation (QAM) [2, 9].

(ii) Using Nyquist-half cycle (NHC) signaling where a rectangular-spectrum shape is adopted for the transmission pulses to ensure zero intersymbol interference (ISI) based on first Nyquist criterion [14, 17, 23-25]. In this case, the minimum transmission bandwidth required to transmit R_s symbol rate with zero ISI is equal to $R_s/2$. In other words, the raised-cosine filter shaping is redesigned here using approximated zero roll-off factor.

(iii) Transmitting only one single-sideband (SSB) of the optical modulated carrier [25, 26-28]. The SSB transmission

* Corresponding author:
mays.monadel23@gmail.com (Mays M. Ibrahim)
Published online at http://journal.sapub.org/ijnc

also reduces the effect of fiber group-velocity dispersion (GVD) which limits the maximum transmission distance in high-bit rate communication fiber link [29, 30].

(iv) Using wavelength-division multiplexing (WDM) [9, 14, 22, 25, 31, 32] and polarization-division multiplexing (PDM) [11, 16, 27]. The PDM uses dual-polarization (DP) transmission to double the transmitted data rate.

Recently, NHC-SSB SCM attracts increasing interest as a high spectral efficiency-modulation scheme suitable for high-bit rate links in short- and medium-reach optical network applications [1, 17, 25, 31]. An optical link based on this modulation scheme can be implemented using IM/DD configuration which reduces the cost and increases the robustness of the link. In 2017, Zhu et al. [23] have demonstrated the transmission of 16-QAM 224 Gbps data over 160 km standard single-mode fiber (SSMF) at C-band using NHC-SSB modulation. The transmission system uses optical carrier-assisted (OCA) technique to enhance the detection efficiency of the used DD receiver. In the experiment, the optical carrier was added with an additional (signal) laser at the transmitter side and the resultant waveform was delivered along the fiber. The scheme is equivalent to heterodyne coherent detection with a local oscillator and a single-ended photodiode (PD). The experimental results of Ref. [23] set a record of fiber link length for C-band 224 Gbps single channel and single PD direct detection transmission. Therefore, the OCA-NHC SSB configuration will be used as a basis for investigation in this work. The aim of is to investigate the transmission performance of NHC-SSB system operating at different link environments. This includes a single-channel and WDM systems operating at C- and O-bands with and without optical amplification using IM/DD scheme.

2. System Configuration and Noise Analysis

2.1. System under Observation

Figure 1 shows a block diagram of the single-channel system under observation. The following remarks should be noted about this system

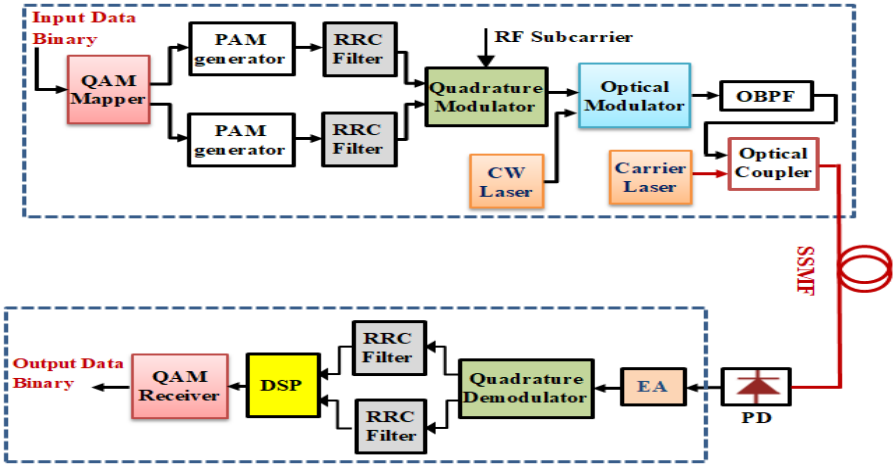

Figure 1. Block diagram of optical-carrier assisted intensity modulation/direct detection (IM/DD) system incorporating Nyquist half-cycle (NHC) single-sideband (SSB) modulation format. PAM: Pulse amplitude modulation; RRC: Root raised-cosine; OBPF: Optical bandpass filter; PD: Photodiode; EA: Electronic amplifier, DSP: Digital signal processing

(i) The system uses IM/DD scheme.

(ii) Ideally, the raised-cosine shaping filters should be designed with zero roll-off factor "r" to match Nyquist pulse shaping (ideal lowpass filter spectrum). Practically, r is set to a small value such as 0.02 to enable efficient filtering process in the next steps. Therefore, the transmission bandwidth is limited to

$$B_T = (1+r)R_s/2 \quad (1a)$$

$$= (1+r)R_b/2log_2M \quad (1b)$$

with r is approximated to zero. Here, R_s is the symbol rate, R_b is the bit rate, and M is the modulation order.

(iii) A high-order optical bandpass filter is used to select the lower-sideband (LSB) of the optical modulator output.

(iv) The system uses two laser sources. A signal laser of frequency f_s which is modulated by the data. The second laser is called the carrier laser of frequency $f_c = f_s + (1+r)R_s/2$ and acts as an assisted carrier. The fields of the modulated signal laser and carrier laser should be combined before optical detection and therefore, the detection process is based on OCA-scheme. This scheme is useful for using DD receiver to detect the optical SSB signal.

(v) The optical receiver uses a digital signal processing (DSP) unit for compensating fiber dispersion and nonlinear optics effects.

(vi) The transmission link consists mainly of a SSMF. If optical amplifiers (OAs) are used to compensate fiber losses, the link is divided into many spans. Each span consists of 50 km SSMF followed by an OA to compensate the span loss.

(vii) The field of the continuous-wave (CW) carrier laser can be combined with the field of the SSB component of the modulated signal laser at the transmitter side. This scheme is

useful since both carrier and signals lasers are under control in the transmitter side. However, in WDM system, the carrier laser may be used in the receiver side to reduce the interference with near neighboring signal channels and also to reduce the effect of fiber nonlinear optics.

2.2. Receiver Noise Analysis

This subsection presents frame work to identify the noise characteristics of the detection process in the receiver. Two special cases are considered here, one corresponds to a transmission link incorporating OAs and the second one corresponds to unamplified link. The first case has been investigated briefly in Ref. [23] and will be discussed again here for comparison purposes with the second case. It is worth to mention here that unamplified links are useful for short-reach optical networks from cost and robustness points of view.

2.2.1. Noise Analysis for Amplified-Link System

This subsection presents detailed derivation of expressions describing the SNR of NHC SSB receiver incorporated in an amplified link system. The derivation stands heavily on the analysis reported in Ref. [23] and gives clear steps with remarks.

The optical signal lunched at the fiber input can be expressed as

$$\boldsymbol{g(t)} = [c(t) + m(t)]\boldsymbol{e_x} \tag{2}$$

where $c(t)$ is the assisted optical carrier and $m(t)$ is the SSB optical signal. The polarization of both $c(t)$ and $m(t)$ are assumed to be aligned along the x axis with $\boldsymbol{e_x}$ denotes the unit vector of the x polarization. Further,

$$c(t) = A_c \exp(j2\pi f_c t) \tag{3a}$$

$$m(t) = A_s\, u(t) \exp[\, j2\pi(f_s - f_{sc})t] \tag{3b}$$

where
A_c= Field amplitude of the CW optical carrier.
f_c= Frequency of the CW optical carrier.
A_s= Field amplitude of the CW optical signal.
f_s= Frequency of the CW optical signal.
f_{sc}= frequency of the RF subcarrier.
$u(t)$= Baseband signal with |u (t)|≤1.

Assume that the optical channel has idea characteristics (i.e., the effect of attenuation, dispersion, and nonlinear optics are negligible) and the receiver performance is dominated by the contribution of amplified spontaneous emission (ASE) noise $\boldsymbol{n(t)}$ generated by the in-line optical amplifiers

$$\boldsymbol{n(t)} = n_x(t)\, \boldsymbol{e_x} + \, n_y(t)\, \boldsymbol{e_y} \tag{4}$$

Here, $n_x(t)$ and $n_y(t)$ denote the ASE noise sources in both polarization and $\boldsymbol{e_y}$ is the unit vector of the y polarization. Under these assumptions, the received optical signal **r(t)** can be written as

$$\boldsymbol{r(t)} = \boldsymbol{g(t)} + \boldsymbol{n(t)} \tag{5a}$$

$$= r_x(t)\, \boldsymbol{e_x} + \, r_y(t)\, \boldsymbol{e_y} \tag{5b}$$

where $r_x(t)$ and $r_y(t)$ are the x and y polarization components, respectively.

$$r_x(t) = A_c \exp(j2\pi f_c t) + A_s u(t) \exp[\, j2\pi(f_s - f_{sc})t] + n_x(t) \tag{6a}$$

$$r_y(t) = n_y(t) \tag{6b}$$

The receiver PD generates a photocurrent $i_{ph}(t)$ which is related to the square of the incident field amplitude

$$i_{ph} = \mathcal{R}\left[|r_x(t)|^2 + \left|r_y(t)\right|^2\right] \tag{7}$$

where $\mathcal{R} = \eta q/hf_0$ is PD responsitivity with is PD quantum efficiency, q is the electron charge, h is Planck's constan, t and $f_0 = f_c \approx f_s$ is the frequency of the incident field.

Inserting eqns. (6a) and (6b) into eqn. (7) yields

$$\begin{aligned} i_{ph}(t) = \mathcal{R}\left|\begin{matrix} A_c \exp(j2\pi f_c t) \\ +A_s\, u(t) \exp[\, j2\pi(f_s - f_{sc})t] + \, n_x(t) \end{matrix}\right|^2 \\ + \mathcal{R}\left|n_y(t)\right|^2 \\ = \, \mathcal{R}\left[A_c^2 + 2A_s A_c \, Re\left\{u(t) \exp\left[j2\pi\left(f_{lf} + f_{sc}\right)t\right]\right\}\right] \\ + A_c^2|u(t)|^2 + \, 2A_c Re\{\exp(-j2\pi f_c t) n_x(t)\} \\ + 2A_s Re\,\{u(t) \exp[j2\pi(f_s - f_{sc})t]\, n_x(t)\} \\ + |n_x(t)|^2 + \left|r_y(t)\right|^2 \end{aligned} \tag{8}$$

where $f_{lf} = |f_c - f_s|$ is the intermediate frequency (f_{lf}) and Re [.] denotes the real part of the complex argument.

To get a clear physical insight on eqn. (8), the photocurrent may splitted into group of components

$$i_{ph}(t) = I_{Dc} + i_s(t) + i_{s\times s}(t) + i_{c\times n}(t) + i_{s\times n}(t) + \, i_{n\times n}(t)$$

$I_{Dc} =$ Dc component.
$i_s(t) =$ Desired signal.
$i_{s\times s}(t)$ =Signal-signal beat interference (SSBI).
$i_{c\times n}(t) =$ Carrier-noise (from the same polarization) beating.
$i_{s\times n}(t) =$ Signal-noise (from the same polarization) beating.
$i_{n\times n}(t) =$ Noise-noise beating.

The expressions of these six photocurrent component are as follows

$$I_{Dc} = \mathcal{R}A_c^2 \tag{9a}$$

$$i_s(t) = 2\mathcal{R}A_s A_c Re\left[u(t) \exp\left\{j2\pi\left(f_{lf} + f_{sc}\right)t\right\}\right] \tag{9b}$$

$$i_{s\times s}(t) = \mathcal{R}A_c^2|\mathrm{u(t)}|^2 \tag{9c}$$

$$i_{c\times n}(t) = 2\mathcal{R}A_s A_c Re\{\exp(-\, j2\pi f_c t)\, n_x(t)\} \tag{9d}$$

$$i_{s\times n}(t) = 2\mathcal{R}A_s Re[u(t) \exp\{j2\pi(f_s - f_{sc})t\} n_x(t)] \tag{9e}$$

$$i_{n\times n}(t) = \mathcal{R}(|n_x(t)|^2 + |n_y(t)|^2) \tag{9f}$$

The electrical signal-to-noise ratio (SNR_e) can be deduced from the photocurrent

$$SNR_e = \frac{P_{Se}}{P_{Ne}} \tag{10}$$

where P_{Se} and P_{Ne} are the average power of the signal and noise associated with the photocurrent, respectively.

$$P_{Se} = E[|i_S(t)|^2] = 2\mathcal{R}^2 A_c^2 A_s^2\, P_u \tag{11a}$$

where $P_u = E[|u(t)|^2]$. Here $E(.)$ denotes the expectation of the argument

$$P_{Ne} = E[|i_{c\times n}(t)|^2] + E[|i_{s\times n}(t)|^2] + E[|i_{n\times n}(t)|^2] = 2\boldsymbol{\mathcal{R}}^2 A_c^2 N_0 B_f + 2\boldsymbol{\mathcal{R}}^2 A_s^2 N_0 B_f + 2 N_0 B_f \quad (11b)$$

Here N_0 is the spectral density of the received ASE noise in each polarization and B_f is the optical band pass filter (OBPF) bandwidth used at the receiver side to suppress the amplified spontaneous emission noise incident on the PD.

Substituting eqns. (11a) and (11b) into eqn. (10) gives

$$SNR_e = \frac{A_c^2 A_s^2 P_u}{(A_c^2 + A_s^2 P_4 + \frac{1}{2}) N_0 B_f} \quad (12)$$

The following remarks can be noted here

(i) The power of the optical carrier $P_{car} = A_c^2$ and the power of the optical signal $P_{sig} = A_s^2 E[|u(t)|^2]$. The carrier-to-signal power ratio is then given by

$$CSR = \frac{P_{car}}{P_{sig}} = \frac{A_c^2}{A_s^2 P_4} \quad (13a)$$

The optical signal-to-noise ratio (OSNR)

$$SNR_0 = \frac{P_c + P_{sig}}{2N_0 B_{ref}} = \frac{[1+CSR]P_{sig}}{2N_0 B_{ref}} \quad (13b)$$

In eqn. (13b), the powers of both signal and carrier are considered with B_{ref} is reference optical bandwidth which is usually set to 0.1 nm in the measurement.

(ii) After the photodetection, the signal-to-SSBI ratio SIR is given by

$$SIR = \frac{P_c}{E[|i_{s\times s}(t)|^2]} = \frac{2\boldsymbol{\mathcal{R}}^2 A_c^2 A_s^2 P_4}{\boldsymbol{\mathcal{R}}^2 A_s^4 P_4^2} = \frac{2A_c^2}{A_s^2 P_4} = \frac{2P_{car}}{P_{sig}} \quad (14)$$

(iii) Consider the special case when the carrier-noise beat dominates the receiver noise. This occurs when $OSNR \ll 1$ and $CSR \ll 1$. Then the electrical SNR can be rewritten as (see eqn. (12))

$$SNR_e = \frac{A_s^2 P_4}{N_0 B_f} = \frac{P_{sig}}{N_0 B_f} = \frac{2 B_{ref}}{B_f} \frac{OSNR}{CSR+1} \quad (15)$$

2.2.2. Noise Analysis for an Unamplified-Link System

The optical signal lunched at the fiber input can be expressed by eqn. (2). The receiver PD generates a photocurrent $i_{ph}(t)$ which is related to the square of the incident field amplitude

$$\begin{aligned} i_{ph}(t) &= \mathcal{R}|c(t) + m(t)|^2 \\ &= \mathcal{R}[|c(t)|^2 + c(t)m^*(t) + c^*(t)m(t) + |m(t)|^2] \\ &= \mathcal{R}[|c(t)|^2 + 2Re\{c(t)\}Re\{m(t)\} \\ &\quad + 2\mathrm{I}_m\{c(t)\}\mathrm{I}_m\{m(t)\} + |m(t)|^2] \\ &= \mathcal{R}[|c(t)|^2 + 2Re\{c^*(t)m(t)\} + |m(t)|^2] \end{aligned} \quad (16)$$

Substituting eqns. (3a) and (3b) into eqn. (16) yields

$$i_{ph}(t) = \mathcal{R}A_c^2 + 2\mathcal{R}A_c A_s\, Re\left[u(t)\exp\{-j2\pi(f_{If} + f_{sc})t\}\right] + \mathcal{R}A_s^2|u(t)|^2 \quad (17)$$

According to eqn. (17), the photocurrent is splitted into three components

$$i_{ph}(t) = I_{Dc} + i_s(t) + i_{s\times s}(t) \quad (18)$$

where $I_{Dc}, i_s(t)$ and $i_{s\times s}(t)$ denote the direct-current (DC) component, desired signal, and SSBI, respectively, which are given by

$$I_{Dc} = \mathcal{R}A_c^2 \quad (19a)$$

$$i_s(t) = 2\mathcal{R}A_c A_s Re[u(t)\exp\{-j2\pi(f_{If} + f_{sc})t\}] \quad (19b)$$

$$i_{s\times s}(t) = \mathcal{R}A_s^2|\mathrm{u(t)}|^2 \quad (19c)$$

Few remarks concerning eqns. (19a) – (19c) are given here

(i) The DC component I_{Dc} can be blocked by inserting a series capacitance in the current path.

(ii) The signal component $i_s(t)$ represents a DSB/suppressed carrier (SC) as a modulated version of the baseband signal $u(t)$ with an effective RF carrier having a frequency equals $(f_{If} + f_{sc})$. Coherent (synchronous) quadrature demodulator should be used to recover the signal $u(t)$ from the component $i_s(t)$.

(iii) The SSBI component $i_{s\times s}(t)$ cannot be eliminated by any filtering process since its spectrum overlaps with the signal spectrum.

The electrical signal-to-noise ratio (SNR_e) associated with the photocurrent can be computed from eqn. (10). In the absence of optical amplification, the main receiver noise components are thermal noise, which is mainly due to the front-end electronic amplifier used to amplify the photogenerated current, carrier shot noise, and signal shot noise [32]

$$P_{ne} = \sigma_{th}^2 + \sigma_{csh}^2 + \sigma_{ssh}^2 \quad (20a)$$

where $\sigma_{th}, \sigma_{csh}$, and σ_{ssh} denote, respectively, the standard deviations (root-mean-square (RMS)) noise currents and they are given by

$$\sigma_{th}^2 = \frac{4K_B T}{R_L} F_n B_e \quad (20b)$$

$$\sigma_{csh}^2 = 2q\mathcal{R}A_c^2 B_e = 2q\mathcal{R}P_c B_e \quad (20c)$$

$$\sigma_{ssh}^2 = 2q\mathcal{R}A_s^2 P_u B_e = 2q\mathcal{R}P_s B_e \quad (20d)$$

Equation (20a) is a well-known expression for the noise associated with electronic amplifier characterized by R_L load resistance and F_n noise figure [33]. In this equation, $K_B = 1.38 \times 10^{-23}$ J/k is Boltzmann constant, T is the absolute temperature (in Kelvin), and B_e is the receiver electrical bandwidth. Equations (20c) and (20d) are deduced from the fact that the power spectral density (PSD) of the shot noise equals ($2q \times$ average current), where q is the magnitude of the electric charge [34].

The electrical SNR of the unamplified-link system is then given by

$$(SNR_e)_u = \frac{2R^2 P_c(L) P_s(L)}{\left[\frac{4K_B T}{R_L} F_n + 2qR P_c(L) + 2qR P_s(L)\right] B_e} \quad (21)$$

where $P_c(L)$ and $P_s(L)$ denote, respectively, the carrier and signal power estimated at the end of the fiber link whose length is L, and they are related to the power launched at the fiber input (P_{co} and P_{so}) by

$$P_c(L) = P_{co}\, e^{-\alpha L} \quad (22a)$$

$$P_s(L) = P_{so}e^{-\alpha L} \quad (22b)$$

Here L is the fiber length in km, α is the fiber power attenuation coefficient measured in km^{-1}, and it is related to fiber loss parameter α_{dB} (measured in dB/km) by

$$\alpha_{dB} = 4.34\ \alpha \quad (23)$$

Equation (21) is then rewritten as

$$(SNR_e)_u = \frac{2e^{-\alpha L}R^2P_{co}P_{so}}{[\frac{4K_BTF_n}{R_L}+2qRe^{-\alpha L}P_{co}+2qRe^{-\alpha L}P_{so}]B_e} \quad (24)$$

Equation (24) is valid when the carrier laser is inserted at the fiber input. Further, the effect of fiber dispersion on degrading the quality of the received optical signal is neglected here. This assumption is justified for dispersion-compensated or dispersion-equalized links.

For the special case corresponding to inserting the carrier laser at the receiver side ($i.e$, the carrier laser field is coupled with the received signal field, and the resultant waveform is applied to the PD), then eqn. (24) can be modified to cover this case

$$(SNR_e)_{ur} = \frac{2e^{-\alpha L}R^2P_{cr}P_{so}}{[\frac{4K_BTF_n}{R_L}+2qRP_{cr}+2qRe^{-\alpha L}P_{so}]B_e} \quad (25)$$

where P_{cr} is the power of the receiver-side inserted CW carrier laser. Here $(SNR_e)_{ur}$ is the electrical SNR corresponding to the case of an unamplified link supported with carrier laser inserted at the receiver side.

3. Results

This section presents results related to NHC-SSB system operating with different transmission link environment. Eight scenarios are used to describe the link environment based on the operating wavelength, number of WDM multiplexed channels, and the presence or absence of optical amplification. These scenarios are

Scenario *A1* : 1310 nm single-channel system without optical amplifiers.

Scenario *A2* : 1310 nm single-channel system with optical amplifiers.

Scenario *A3* : O-band WDM system without optical amplifiers.

Scenario *A4* : O-band WDM system with optical amplifiers.

Scenario *B1* : 1550 nm single-channel system without optical amplifiers.

Scenario *B2* : 1550 nm single-channel system with optical amplifiers.

Scenario *B3* : C-band WDM system without optical amplifiers.

Scenario *B4* : C-band WDM system with optical amplifiers.

A 224 Gbps 16-QAM data is assumed to be carried by each single channel. Other parameters valued used in the simulation are listed in Table 1. The values of maximum transmission distance L_{max} reported in this section correspond to the lengths of the fiber link which make the receiver bit error rate (BER) approaches its threshold value. A 4.5×10^{-3} BER threshold is used here which corresponds to 7% overhead hard-decision (HD) forward-error correcting (FEC). The simulation results are obtained using Optisystem ver. 14 software package.

Table 1. System parameters values used in the simulation for the NHC-SSB system operating with 224 Gbps 16-QAM signaling. The blue- and red-color numbers are corresponding to 1550 nm 1310 nm systems, respectively

Subsystem	Component	Parameter	Value
Transmitter	Signal laser	Frequency f_s	228.85 THz 193.1 THz
	Carrier laser	Frequency f_c	228.87856 THz 193.12856 THz
	Mach-Zehnder optical modulator	Loss	2 dB
	Optical SSB filter	Center frequency	228.82144 THZ 193.07144 THz
		Bandwidth	56 GHZ
Optical link	Fiber (SSMF)	Attenuation α	0.35 dB/km 0.2 dB/km
		Dispersion D	0 16.75 ps/nm/km
		Dispersion slop S	0.092 ps/nm^2/km 0.075 ps/nm^2/km
		Effective area	93 um^2 80 um^2
		Nonlinear index coefficient n_2	26×10^{-21} m^2/W
Receiver	Photodiode	Responsibility $\mathcal{R}$	1 A/W
	Front-end electronic amplifier	Load resistance R_L	3.3 kΩ
		Noise Figure F_n	4.8 dB

3.1. Single-Channel Transmission

Figure 2 shows the signals spectra and constellation diagrams at different points of the unamplified 1310 nm single-channel system (Scenario A1). The results are obtained using $P_s = 0$ dBm, $P_c = 0$ dBm (inserted at the transmitter side) and fiber length L =36 km. This link length corresponds to the maximum transmission distance, L_{max}, under these conditions. Note that the a double-side band (DSB) spectrum of the modulated radio frequency (RF) subcarrier covers approximately 56 GHz bandwidth which corresponds to $2[(1+r)R_s/2] \cong R_s$ when $r \approx 0$. This 56 GHz bandwidth also equals the bandwidth of the transmitted optical SSB signal. Note further, the ability of used DSP unit to compensate the fiber dispersion and recover the required constellation diagram. The simulation is repeated for the unamplified 1550 nm single-channel system (Scenario $B1$) and the results are reported in the Appendix.

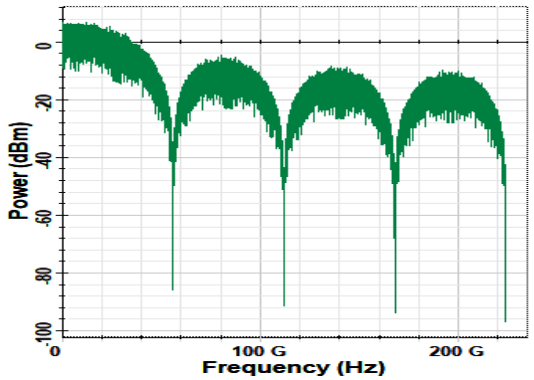

(a)

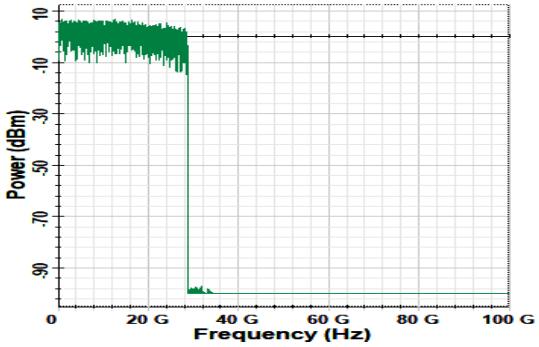

(b)

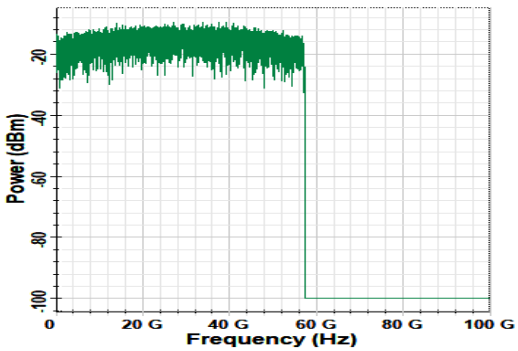

(c)

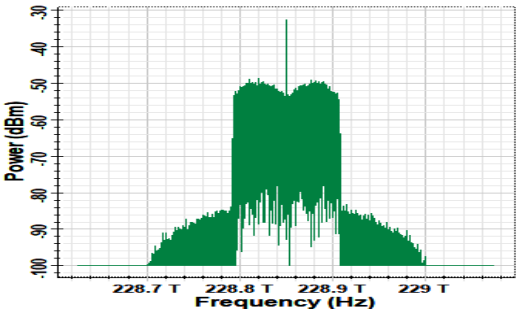

(d)

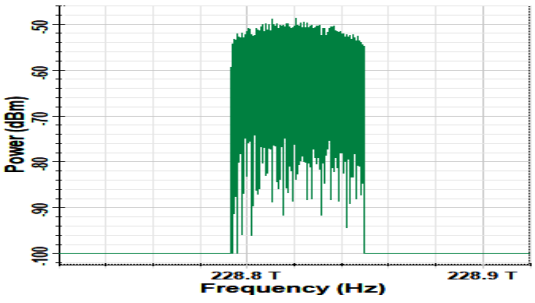

(e)

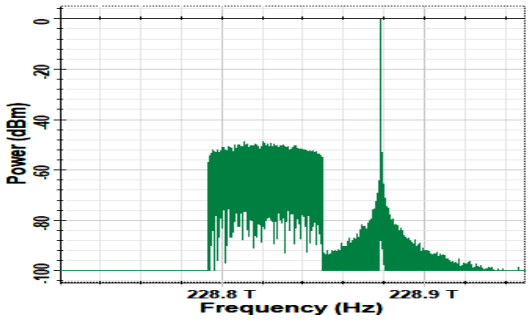

(f)

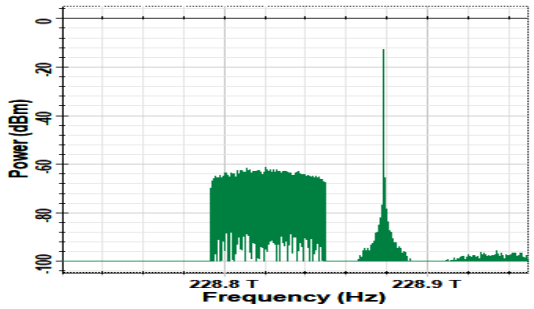

(g)

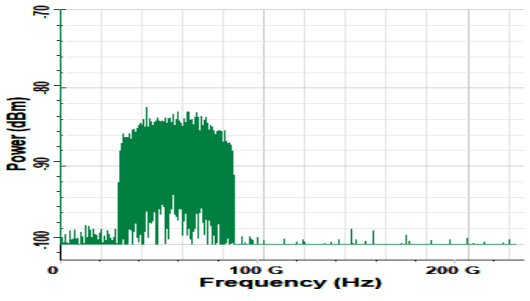

(h)

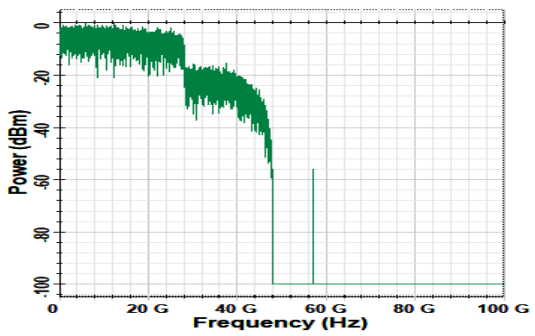

(i)

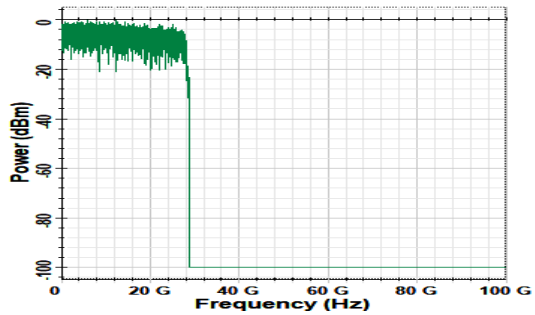

(j)

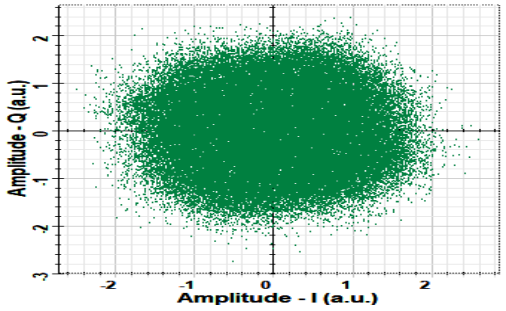

(k)

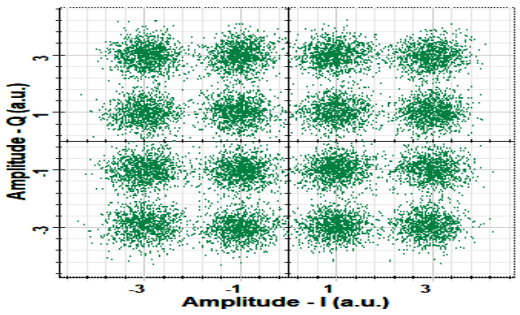

(l)

Figure 2. Spectra and constellation diagrams related to an unamplified link 224 Gbps 16-QAM system operating at 1310 nm wavelength with L=36 km, P_s=0 dBm and P_c=0 dBm (carrier at transmitter). (a) Spectrum of the QAM pulse generator output (I-phase component). (b) Spectrum of the QAM modulator input. (c) Spectrum of the QAM modulator output. (d) Spectrum of the optical modulator output. (e) Spectrum of the optical SSB signal. (f) Spectrum of signal SSB + assisted carrier. (g) Spectrum of the optical signal at the fiber output. (h) Spectrum of the amplified photocurrent. (i) Spectrum of the QAM demodulator output. (j) Spectrum of the filtered QAM demodulator output. (k) Receiver constellation diagram at the DSP input. (L) Receiver constellation diagram at the DSP output

Figures 3a and b compare the maximum transmission distance achieved by the unamplified 1310 and 1550 nm systems when the carrier is inserted at the transmitter or receiver side, respectively. Results related to amplified single-channel systems are presented in Figs. 4a and 4b. In both Figs. 3 and 4, the carrier laser power P_c is set to 0 dBm, and the values of L_{max} are estimated for different values of signal laser power P_s.

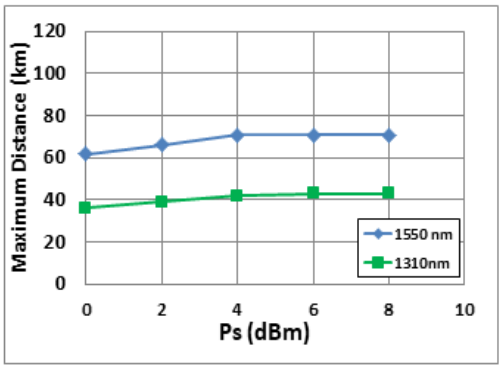

(a)

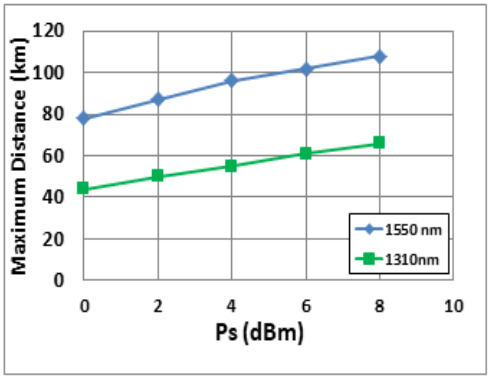

(b)

Figure 3. Variation of maximum reach L_{max} with signal laser power P_s assuming **unamplified** 224 Gbps 16-QAM system operating with $P_c = 0$ dBm. (a) Carrier at the transmitter. (b) Carrier at the receiver

Investigating the results in Fig. 3a and 3b reveals the following findings

(i) Moving the laser carrier from the transmitter side to the receiver side increases the maximum transmission distance by approximately 30%. In other words, $(L_{max})_R/(L_{max})_T \approx 1.3$ where the subscripts R and T denote that the the carrier laser is inserted in the transmitter and receiver side, respectively. This conclusion is true for both 1310 and 1550 nm systems.

(ii) $(L_{max})_{1550nm}/(L_{max})_{1310nm} \approx 1.7$ independent of the location of the carrier laser. This results indicate clearly that the systems performance is affected mainly by fiber loss and not by dispersion. Recall that the fiber GVD, D is almost negligible at 1310 nm. Further the DSP is used to compensate fiber dispersion and this is more pronounced at 1550 nm where D ≈ 16.75 ps/(nm . km). Note that the values of fiber loss used in the simulation are 0.35 and 0.2 dB/km at 1310 and 1550 nm, respectively. The ratio between the two losses is 1.75 and this is in agreement with the enhancement

of L_{max} achieved at 1550 nm compared with 1310 nm counterpart.

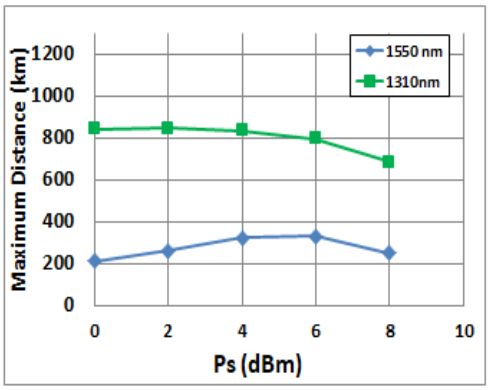

(a)

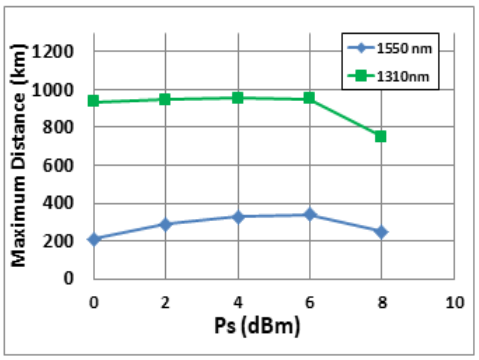

(b)

Figure 4. Variation of maximum reach L_{max} with signal laser power P_s assuming **amplified** 224 Gbps 16-QAM system operating with $P_c = 0$ dBm. (a) Carrier at the transmitter. (b) Carrier at the receiver

The results in Figs. 4a and 4b highlight the following findings

(i) The L_{max}-P_s characteristics is divided into two regions controlled by a critical level of P_s (denoted here by $(P_s)_{critical}$). When $P_s < (P_s)_{critical}$, L_{max} increases slightly with P_s. In contrast, L_{max} decreases strongly with P_s when $P_s > (P_s)_{critical}$ and this behavior comes from the effect of increasing the level of signal-signal beat interference. The values of $(P_s)_{critical}$ are about 6 dBm and 8 dBm for 1310 nm and 1550 nm systems, respectively.

(ii) $(L_{max})_R/(L_{max})_T \approx 1.1$ and 1 for the 1310 and 1550 nm system, respectively, when $P_s < (P_s)_{critical}$

(iii) At P_s =0 dBm, $(L_{max})_{1310nm}/(L_{max})_{1550nm} \approx 4$ and 4.5 when the carrier laser is inserted at the transmitter or receiver, respectively. These values to be compared with 2.6 and 3 when P_s increases to 4 dBm. This enhancement in the maximum transmission distance of the 1310 nm amplified link is expected since the system operates with zero GVD and effectively negligible fiber loss (i.e., loss-compensated link).

3.2. WDM Systems

Two NHC-SSB WDM systems are designed in Optisystem environment for O-band and C-band operation. Each of the WDM system uses 100 GHz channel spacing Δf and carries 224 Gbps 16-QAM date rate per channel. The frequency of ith channel laser is computer from

$$f_i(THz) = \begin{Bmatrix} 193.1 + [i - (1 + N/2)]\Delta f(THz) \\ 228.85 + [i - (1 + N/2)]\Delta f(THz) \end{Bmatrix}$$

Figure 5 shows the spectrum of the O-band multiplexed signal at the fiber input and after 43 km transmission over unamplified link. The results are presented for $P_s = 0$ dBm, $P_c = 0$ dBm (inserted at the receiver side, L=L_{max}=43 km, and $N = 32$). Note that the output spectrum is almost a copy of the input spectrum indicating the absence of distortion due to four-wave mixing (FWM) associated with fiber nonlinear optics. The only difference is the output spectrum level is reduced by 15 dB (=0.35dB/km ×43 km) due to fiber loss. The simulation results in Fig. 5 is repeated in Fig. 6 for $P_s = 8$ dBm and L_{max}=63 km. Note that the spectrum at the fiber output is slightly distorted when compared with the spectrum at the fiber input. This distortion comes from the FWM effect.

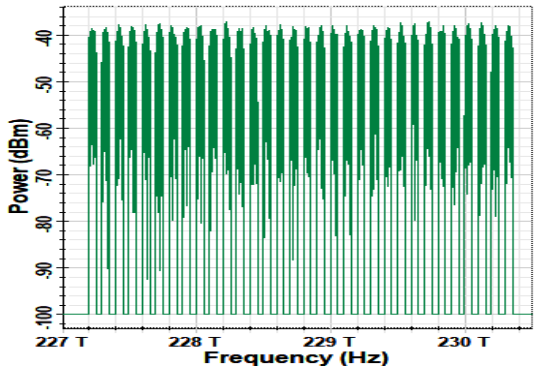

(a)

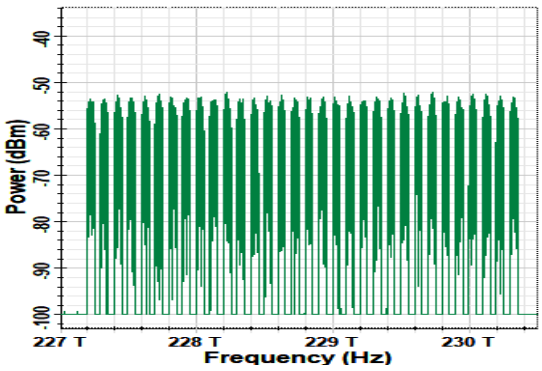

(b)

Figure 5. Optical power spectra corresponding to **unamplified** 32×224 Gbps **O-band** WDM system operating with 16-QAM signal and $P_s = 0$ dBm. (a) At the fiber input. (b) After 43 km transmission

The simulation is carried further to investigate the C-band multiplexed signal spectrum. The results are given in Fig. 7 and 8 assuming $P_s = 0$ and 8 dBm, respectively. The fiber length is set to Lmax which equals $L = 65$ and 60 km, respectively. Other parameters used in the simulation are $P_c = 0$ dBm and $N = 32$. Note that the effect of FWM on the output spectrum is more pronounced when compared with Fig. 5 and 6, especially, when $P_s = 8$ dBm.

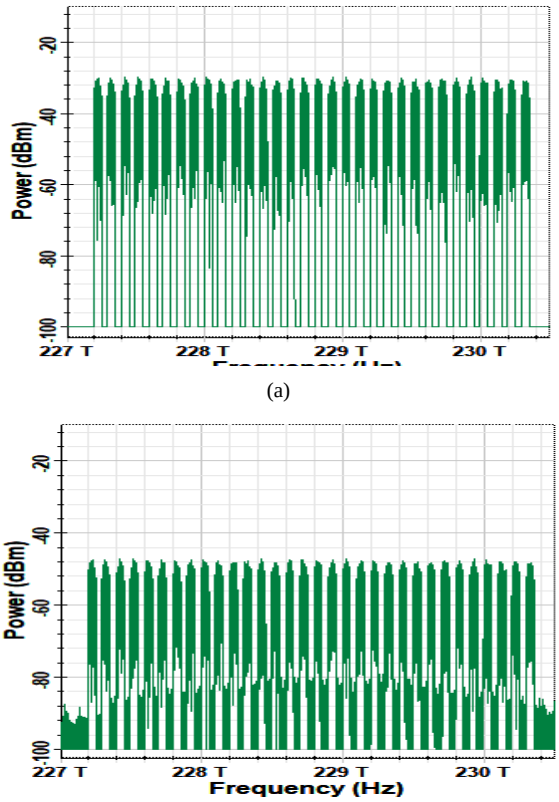

(a)

(b)

Figure 6. Optical power spectra corresponding to **unamplified** 32×224 Gbps **O-band** WDM system operating with 16-QAM signal and $P_s = 8$ dBm. (a) At the fiber input. (b) After 63 km transmission

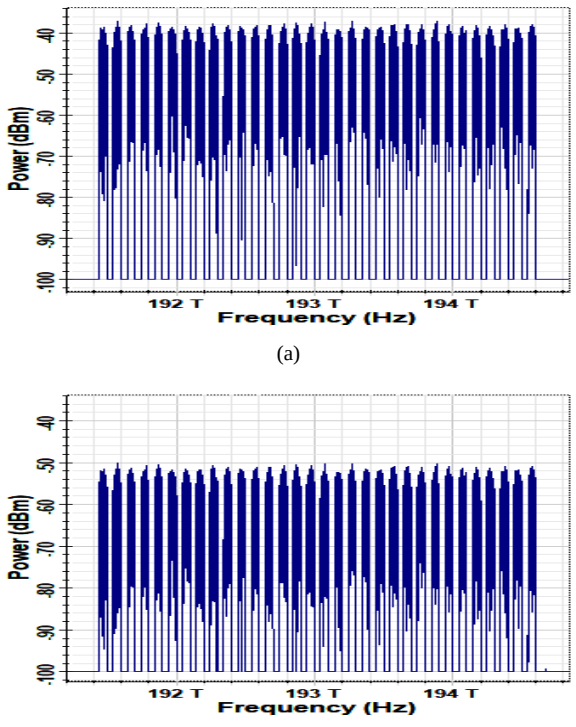

(a)

(b)

Figure 7. Optical power spectra corresponding to **unamplified** 32×224 Gbps **C-band** WDM system operating with 16-QAM signal and $P_s = 0$ dBm. (a) At the fiber input. (b) After 65 km transmission

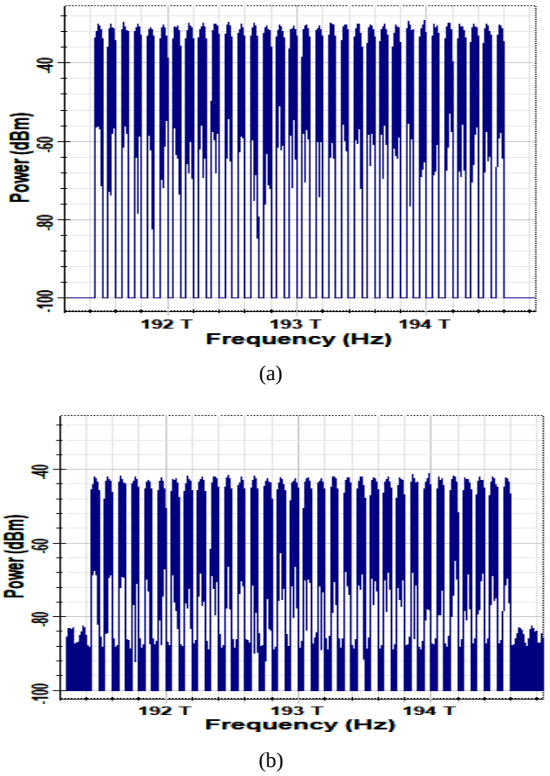

(a)

(b)

Figure 8. Optical power spectra corresponding to **unamplified** 32×224 Gbps **C-band** WDM system operating with 16-QAM signal and $P_s = 8$ dBm. (a) At the fiber input. (b) After 60 km transmission

Figures 9a and 9b show the dependence of L_{max} onnumber of multiplexed channels for O-band and C-band, respectively. The results are reported for unamplified link with $P_c = 0$ dBm (inserted at the receiver side). The O-band operation reveals the following results

(i) When the number of multiplexed channels $N \leq 16$, the maximum transmission distance is almost independent of N. Further, L_{max} increases with signal laser power P_s. When P_s=0 dBm, $L_{max} \approx 44$ km when N= 1, 4, 8, and 16. Increasing P_s to 10 dBm yields $L_{max} \approx 68$ km.

(ii) Increasing N to 32 decreases L_{max} to 43 km and 50 km, when P_s=0 and 10 dBm, respectively. Note also that L_{max} increases with P_s and reaches 63 km when P_s=8 dBm. Increasing P_s above 8 dBm reduces the value of L_{max}. This behavior can be attributed to FWM effect associated with fiber nonlinear optics. Therefore, one can conclude that the optimum value of P_s=8 dBm when N=32 which gives the longest possible reach of 63 km.

Investigating the results of the C-band operation (Fig. 9b) highlights the following conclusions

(i) L_{max} is almost independent of N when $N \leq 8$. When P_s = 0 dBm, L_{max}= 78, 77, and 75 km when N= 1, 4, and 8, respectively. Increasing P_s to 8 dBm will increase L_{max} to 108 km for these three values of N.

(ii) Increasing N to 16 and 32 reduces L_{max} and this effect is more pronounced for high values of P_s. At P_s=0 dBm, L_{max} = 72 and 65 km when N= 16 and 32, respectively. These values are to be compared with 90 and 60 km when P_s=8 dBm, respectively.

(iii) The optimum values of P_s which give the longest possible reach are 8 and 4 dBm for N= 16 and 32, respectively. The corresponding values of L_{max}= 90 and 77 km, trspectively.

The transmission performance of the amplified WDM system is also investigated for both O-band and C-band operation. Here only brief results are given corresponding to the special case of P_s= P_c= 0 dBm. The results reveal that the O-band system offers L_{max}= 935, 650, 560, and 450 km for N= 1, 4, 8, and 16, respectively. These results highlight the effect of FWM which is more pronounced in low dispersion fiber. The C-band system gives L_{max}= 210, 210, 210, and 110 km for N= 1, 4, 8, and 16, respectively. The results indicate clearly that effect of FWM plays a key role in reducing the performance 0f 16-channel system.

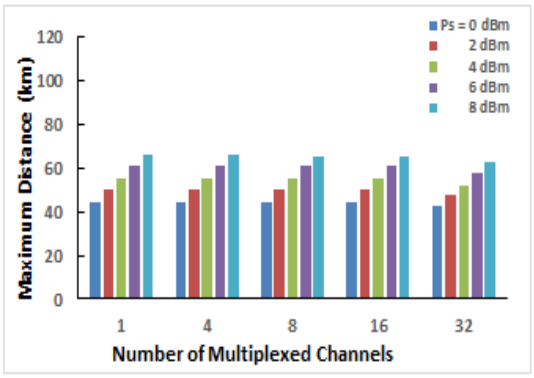

(a)

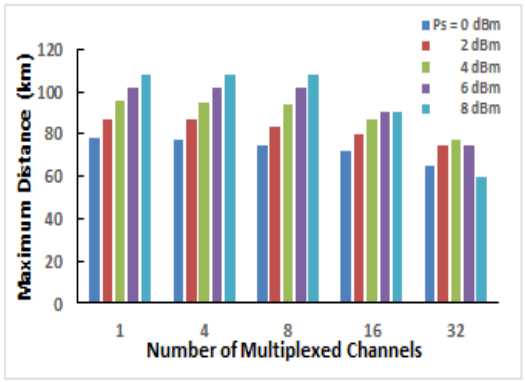

(b)

Figure 9. Dependence of maximum reach of **unamplified** 16-QAM WDM system on number of multiplexed channels and assuming P_c = 0 dBm and 224 Gbps 16-QAM channel data. (a) **O-band**. (b) **C-band**

4. Comparison with Published Experimental Works

4.1. 1550 nm Single-Channel System

This subsection compares simulation results obtained in this work with the experimental data reported in Ref. [23]. Both simulation and experimental results are related to OCA-SCM operates with 224 Gbps NHC-SSB 16-QAM signaling. The experimental results in Ref. [23] were presented for three transmission links: B2B, one span, and two spans. Each span consists of 80 km SSMF ended with 16 dB EDFA for losses compensation. Also an EDFA was inserted at the fiber input to boost the lunch power. The gain *G* of this OA was adjusted to achieve the required lunch power (see Fig. 10).

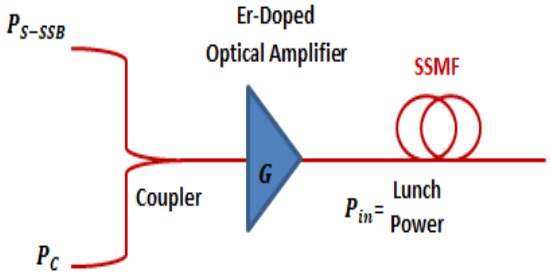

Figure 10. Configuration of an optical link with boost erbium-doped optical amplifier used in the experiment of Ref. [23]

The lunch power P_{in} and the optical carrier-to-signal power ratio (CSPR) were taken as independent parameters in the results presented in Ref. [23]. From Fig.10. The optical signal lunched at the fiber input can be expressed as

$$\text{CSPR} = \frac{P_c}{P_{s-SSB}} \tag{26a}$$

$$P_{in} = GP_{s-SSB} + GP_c \tag{26b}$$

This system is simulated in this work using the following steps

(i) Set the signal laser power P_s to a certain value, simulate the optical modulator subsystem, and record the SSB signal power P_{s-SSB}.

(ii) Calculate the required carrier laser power (P_c = CSPR P_{s-SSB}) and EDFA gain [$G = P_{in}/(P_{s-SSB} + P_c)$].

(iii) Set the values of other system parameters related to the transmitter, transmission link, EDFAs, and receiver as those reported in Ref. [23].

For example, to achieve P_{in} =9 dBm and CSPR = 14 dB as considered in the reference, the signal laser power is set to 5 dBm in the simulation. The simulation yields $P_{s-SSB} = -10.5$ dBm, and therefor, the carrier laser power is set to 3.5 dBm to achieve CSPR = 14 dB. The total power at the coupler output equals $P_{s-SSB} + P_c = 10^{(-10.5/10)} + 10^{(3.5/10)} = 0.09 + 2.24 = 2.33\ mW$, which corresponds to $10\log(2.33) = 3.7$ dBm. The gain *G* of the boost EDFA is set to 5.3 dB to get a 9 dB lunch power. Under these settings, the simulation yields BERs of 4.6×10^{-5}, 2.5×10^{-4}, and 1.3×10^{-3} for B2B, one span, and two-span transmission respectively. These are to be compared with 3×10^{-4}, 2.2×10^{-3}, and 3.6×10^{-3} experimental BERs, respectively, as reported in Fig. 9c in Ref. [23]. Note that, both simulation and experimental BERs are lower than 4.5×10^{-3}, which represents the BER threshold for 7% HD-FEC code. Note further that the simulation BERs, BER_{Sim}, are in the same order of the experimental ones, BER_{Exp} where $\log(BER_{Sim}/BER_{Exp}) \approx 1.25$. Figures 11 (a-c) show the simulated optical spectra after 0, 80, and 160 km transmission distance, respectively.

The simulated and experimental constellation diagrams after 80 and 160 km are given in parts d and e of this figure.

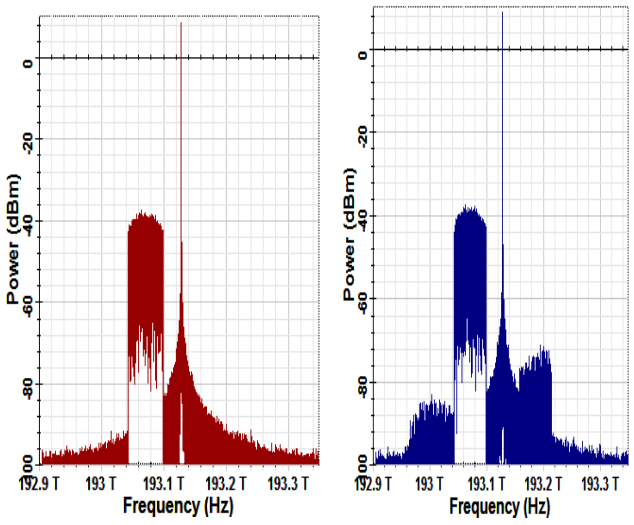

(a) (b)

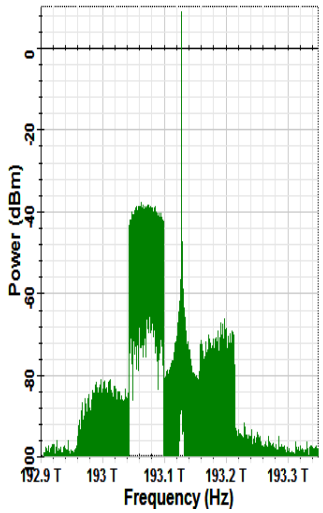

(c)

Figure 11. Spectra of (carrier + SSB) waveforms and constellation diagrams related to **amplified** 224 Gbps carrier-assisted 16-QAM system operating at **C-band** (carrier at transmitter). (a) Spetrum after 0 km transmission. (b) Spectrum after 80 km transmission. (c) Spectrum after 160 km transmission. (d) Simulated and experimental constellation diagrams after 80 km transmission. (e) Simulated and experimental constellation diagrams after 160 km transmission

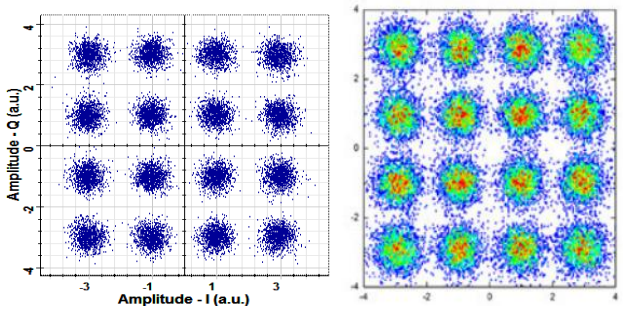

Simulation Experimental

(d)

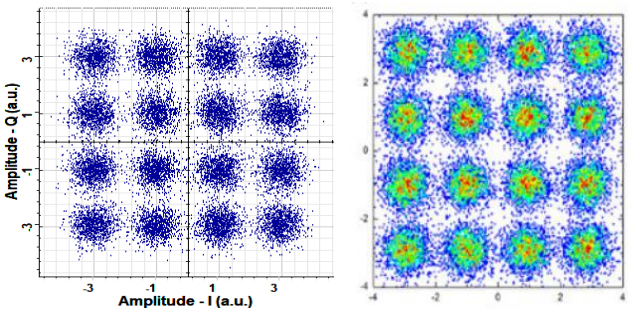

Simulation Experimental

(e)

Figure 11. (Continued)

Figure 12 shows the variation of BER with lunch power after 160 km transmission with CSPR of 14 dB. The marks and in this figure correspond to the simulation results and experimental data, respectively. The experimental results are deduced from Fig. 8 in Ref. [23]. Investigating the results in this figure reveals that both simulation and experiment predict an optimum lunch power of 9 dB.

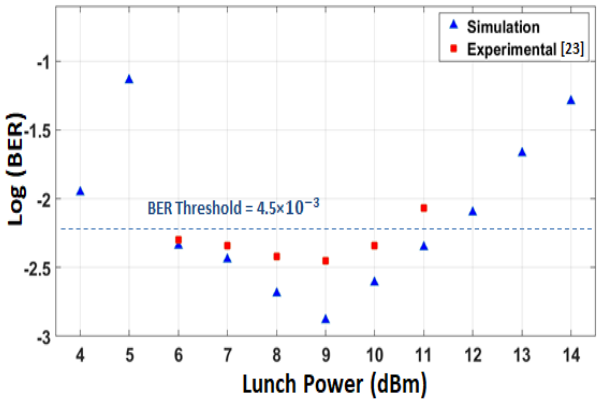

Figure 12. Variation of BER with lunch power after 160 km transmission with CSPR of 14 dB

4.2. C-Band Wavelength-Division Multiplexing System

Zou at al. [28] reported experimental results describing the transmission of 8×100 Gbps WDM signal over 320 km SSMF at C-band. Each channel operates with NHC-SSB 16-QAM signaling and DD scheme. The 320 km distance is distributed into four spans; each span uses 80 km-SSMF followed by 16 dB EDFA for loss compensation. The polarization of the odd lasers (lasers 1, 3, 5, and 7) are set orthogonal to the polarizations of the even lasers (laser 2, 4, 6, and 8) to reduce the interference between successive lasers fields due to fiber nonlinear optics. The WDM system uses 50 GHz channel spacing with additional EDFA inserted after the multiplexer to determine the required total power lunched into the fiber.

Two BER thresholds were used in Ref. [28] to assess the performance of the demonstrated system; 6.73×10^{-3} and 4.5×10^{-3}, which are related to 20% and 7% HD-FEC codes, respectively. Chromatic-dispersion compensation (CDC) technique was used to compensate fiber dispersion. The

experiment was repeated with digital back propagation (DBP) technique to compensate both fiber dispersion and fiber nonlinearity.

To simulate the experimental system reported in [28], an assisted optical carrier is inserted in each of the WDM channel transmitters. Thus, each transmitter contains both signal and carrier lasers. This approach has two main effects. (i) The total power launched into the fiber will be increased leading to high fiber nonlinear optics effects. (ii) The spectrum of the signal at the output of the channel transmitter covers frequencies from $f_L = f_s - (1+r)R_s$ to $f_h = f_c = f_s + 0.5(1+r)R_s$. For $R_b = 100$ Gbps and 16-QAM signaling ($i.e.,$ $R_s = 25$ Gbps) and $r = 0.02$, the bandwidth of the transmitter signal $= f_h - f_L = 1.5(1+r)R_s = 38.25$ GHz. Therefore, channel spacing of 50 GHz with high-order 40 GHz demultiplexer bandpass filters are used to ensure negligible crosstalk in accord with the experimental results.

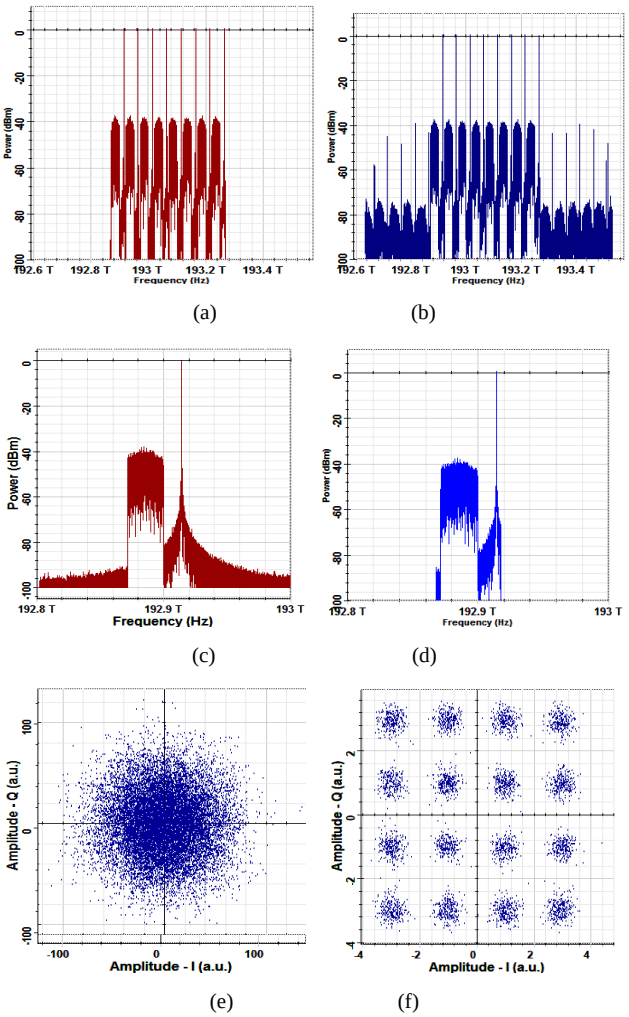

Figure 13. Optical power spectra and constellation diagrams corresponding to **unamplified** (8×100 Gbps) **C-band** WDM system operating with 16-QAM signal and $P_s = 0$ dBm. (a) Spectrum at the fiber input. (b) Spectrum after 320 km transmission. (c) Spectrum at the transmitter output of channel 1. (d) Spectrum at the receiver input of channel 1. (e) Receiver constellation diagram at the DSP input. (f) Receiver constellation diagram at the DSP output

For comparison purposes, the above experimental work is simulated here using Optisystem software with lunch power per channel P_{ch} of 1 dBm and $CSPR$ of 10.2 dB. When P_s is set to 0 dBm, the simulation gives $P_{s-SSB} = -10.5$ dBm $= 10^{(-10.5)/10} = 89\ \mu W$. The carrier laser power P_c required to achieve a $CSPR$ of 10.2 dB is equals -0.3 dB $= [P_{s-SSB}(\text{dBm}) + CSPR(\text{dB})]$. The lunch power per channel $P_{ch} = G(P_{s-SSB} + P_c)$, where G is the gain of the OA inserted after the multiplexer. Note that, $P_{s-SSB} + P_c = 1.022\ mW = 0.095$ dBm. Therefore, $G = 0.905$ dB is used to yield $P_{ch} = 1$ dBm.

Figure 13 shows simulation results related to the system under observation when the transmission link consists of 4 spans (320 km). Parts a and b display the optical spectra at the input and output of the transmission link. Note, the output spectrum contains many intermodulation distortion components due to the effect of fiber nonlinearity. Parts c and d compare the power spectra at the transmitter output and receiver input of channel 1. The two spectra contain almost the same frequency content, which reflects the effectiveness of the receiver DSP unit in compensating chromatic dispersion and nonlinear fiber optics. This is clear further by comparing the constellation diagrams at the receiver before and after the DSP unit as shown in parts e and f of this figure, respectively.

Figure 14 compares the measured BERs [15] and simulated ones for of all the 8 channels after 320 km transmission. Note that the simulated results show BERs lower than the measured values, and hence, confirms the possibility of 320 km transmission even when BER threshold of 4.5×10^{-3} is used. In fact, the simulation predicts successful transmission over 5 spans (400 km) as shown in Fig. 15 when $P_{ch} = 1$ dBm and CSPR= 10.2 dB. Figures 15 also contains results corresponding to CSPR of 8.2 and 12.2 dB and included here to address the effect of CSPR or the channels BERs. Investigating the results in Fig. 4.13 reveals that at constant lunch power per channel ($P_{ch} = 1$ dBm), using CSPR of 10.2 dB offers BERs less than the BER threshold for all the eight channels. Increasing CSPR on 12.2 dB or reducing CSPR to 8.2 dB increases the BERs of the channels and makes some of them above the BER threshold. This result can be explained as follows. $P_{ch} = P_{s-SSB} + P_c = P_{s-SSB}[1 + CSPR]$. Therefore, $P_{s-SSB} = P_{ch}/[1 + CSPR]$, and hence, increasing CSPR leads to increasing P_{s-SSB}. The BER characteristics depends on the effective SNR, which can be stated as

$$SNR_{eff} = \frac{B_0\, P_c\, P_{s-SSB}}{B_1 + B_2\, P_{s-SSB}^2} \tag{27}$$

where the detected electrical signal strength is proportional to the product term (P_{ch} . P_{s-SSB}). In this equation, B_0 is proportionality constant, B_1 represents the signal-independent noise power, and $B_2\ P_{s-SSB}^2$ represents the signal × signal beat interference. Taking the derivative of SNR_{eff} with respect P_{s-SSB} and set it to zero yields

$$B_0\,(B_1 + B_2\, P_{s-SSB}^2)P_c - B_0\, P_{s-SSB}(2B_2\ P_{s-SSB}) = 0$$
$$(P_{s-SSB})_{opt} = (B_1/B_2)^2$$

$$(\text{CSPR})_{opt} = [P_{ch}/P_{s-SSB}]_{opt}$$
$$= P_{ch}(B_2/B_1)^{1/2} - 1$$

Note that, the optimum value of CSPR depends on channel lunch power P_{ch} and system parameters (B_1 and B_2). If one considers a 10.2 dB is the optimum value of CSPR at $P_{ch} = 1$ dB, then $(P_{s-SSB})_{opt} = P_{ch}/[1 + (CSPR)_{opt}] = 1.26/[1 + 10.47] = 0.11\,mW = 110\,\mu W$. Thus, the actual P_{s-SSB} generated by the optical modulator ($= 0.089\,mW$) should by amplified by $110/89 = 1.24 (= 0.93$ dB) before lunching it into the fiber.

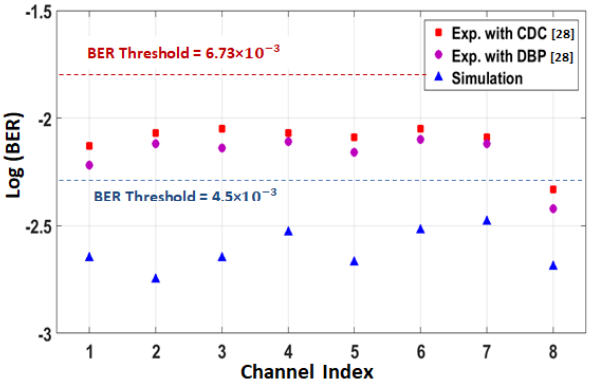

Figure 14. Comparison between measured BERs [28] and simulated ones for all the 8 channels after 320 km transmission assuming $P_{ch} = 1$ dBm and CSPR= 10.2 dB

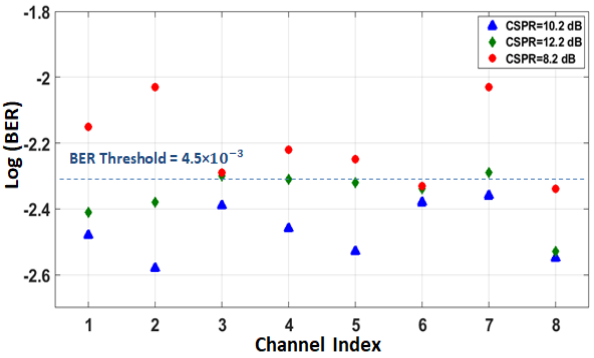

Figure 15. Simulated BERs of the 8 channels after 400 km transmission assuming $P_{ch} = 1$ dBm

5. Conclusions

The noise characteristics and transmission performance have been investigated of optical carrier assisted NHC-SSB system designed with IM/DD scheme. Simulation results have been presented for both amplified and unamplified WDM systems operating at O- and C-bands with 224 Gbps 16-QAM channel data. The simulation results are in good agreement with published experimental data. The main conclusions drawn from this study are

(i) The C-band WDM system offers higher transmission distance compared with O-band counterpart when no optical amplification is used. When P_s=P_c= 0 dBm, L_{max} = 78 and 72 km when number of multiplexed channels N= 1 and 16, respectively, in the C-band system. These values are to be compared with 44 km for O-band system.

(ii) Using optical amplification to compensate the link losses will increase the transmission distance of the C-band WDM system to 210 and 110 km when N= 1 and 16, respectively, and assuming P_s=P_c= 0 dBm. These values are to be compared with 935 and 450 km for the O-band system, respectively.

(iii) Performance degradation due to fiber nonlinear optics becomes effective when N= 32 channels and this is more pronounced when P_s increases beyond 0 dBm. This leads to an optimum value for P_s which gives the longest transmission distance. For the unamplified system, $(P_c)_{optimum}$= 4 and 8 dBm for C- and O-bands, respectively. The corresponding values of L_{max} are 77 and 63 km, respectively.

Appendix

Results Related to 1150 nm Single-Channel Transmitter

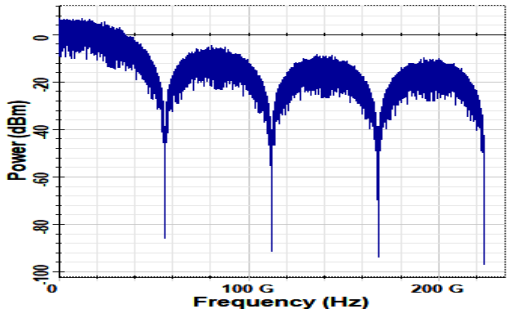

(a)

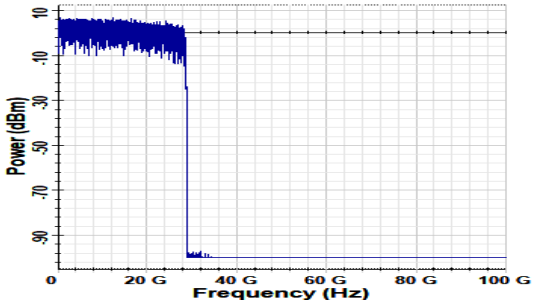

(b)

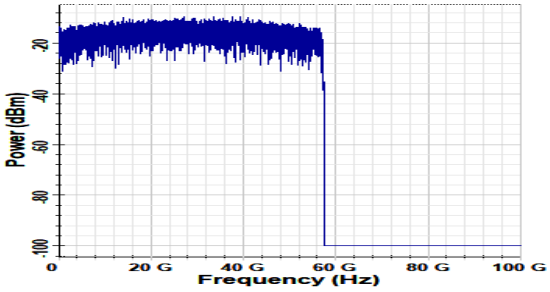

(c)

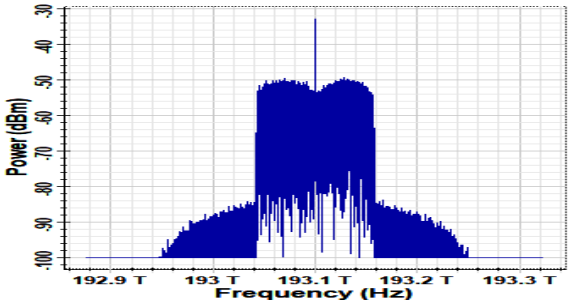

(d)

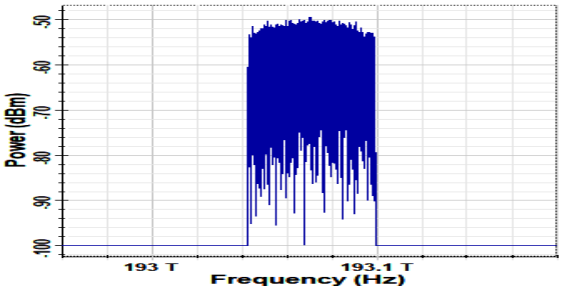

(e)

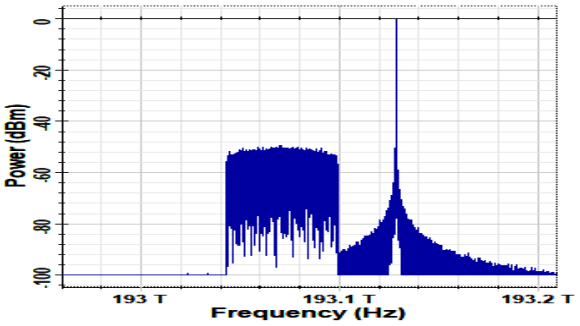

(f)

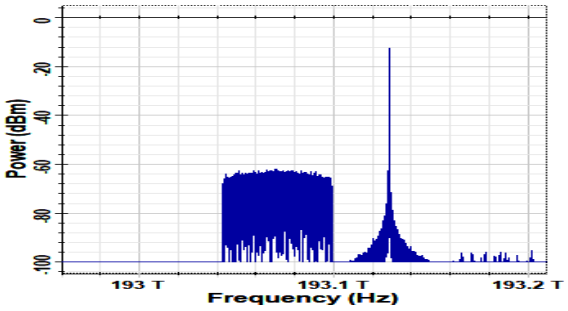

(g)

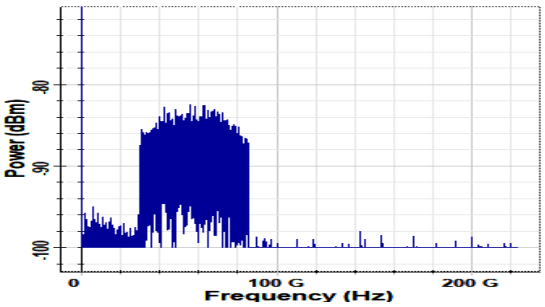

(h)

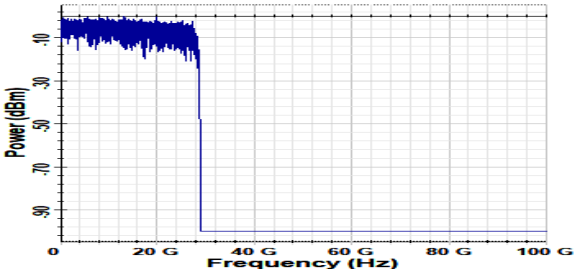

(i)

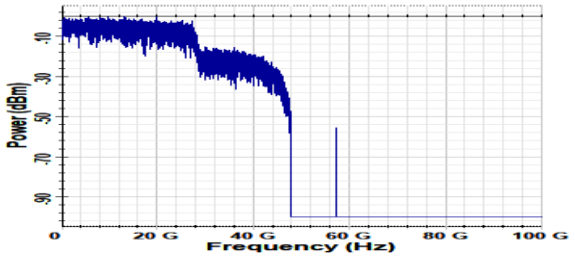

(j)

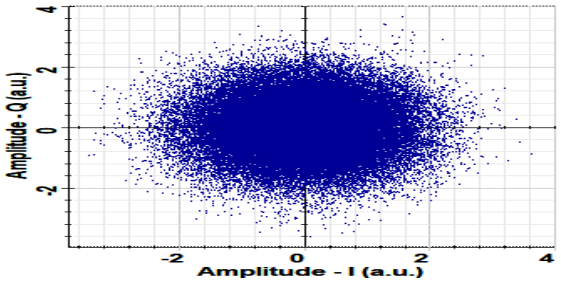

(k)

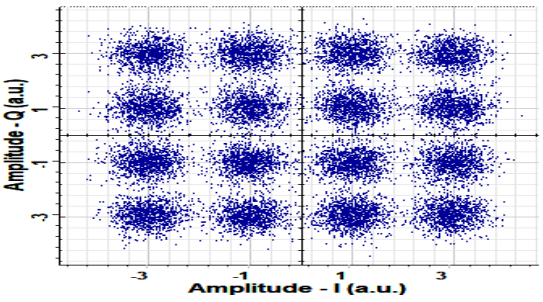

(l)

Figure 16. Spectra and constellation diagrams related to an **unamplified** 224 Gbps 16-QAM system operating at 1550 nm wavelength with L=62 km, P_s=0 dBm and P_c=0 dBm (carrier at transmitter). (a) Spectrum of the QAM pulse generator output (I-phase component). (b) Spectrum of the QAM modulator input. (c) Spectrum of the QAM modulator output. (d) Spectrum of the optical modulator output. (e) Spectrum of the optical SSB signal. (f) Spectrum of signal SSB + assisted carrier. (g) Spectrum of the optical signal at the fiber output. (h) Spectrum of the amplified photocurrent. (i) Spectrum of the QAM demodulator output. (j) Spectrum of the filtered QAM demodulator output. (k) Receiver constellation diagram at the DSP input. (L) Receiver constellation diagram at the DSP output

REFERENCES

[1] J. Zhang, Y. Zheng, X. Hong, and C. Guo, "Increase in capacity of an IM/DD OFDM PON using super-Nyquist

image-induced aliasing and simplified nonlinear equalization", IEEE Journal of Lightwave Technology, vol. 35, no. 19, pp. 4105-4113, Oct. 2017.

[2] O. A. Sab, P. Plantady, A. Calsat, S. Dubost, L. Schmalen, V. Letellier, and J. Renaudi, "25.4-Tb/s transmission over transpacific distances using truncated probabilistically shaped PDM-64QAM", IEEE Journal of Lightwave Technology, vol. 36, no. 6, pp. 1354-1361, Mar. 2018.

[3] A. Tanaka, S. Murakami, T. Tajima, T. J. Xia, and G. A. Wellbrock, "Terabit/s Nyquist super channels in high capacity fiber field trials using DP-16QAM and DP-8QAM modulation formats", IEEE Journal of Lightwave Technology, vol. 32, no. 4, pp. 776-782, Feb. 2014.

[4] R. Linden, N. C. Tran, E. Tangdiongga, and T. Koonen, "Optimization of flexible non-uniform multilevel PAM for maximizing the aggregated capacity in PON deployments", IEEE Journal of Lightwave Technology, vol. 36, no. 12, pp. 2328-2336, Jun. 2018.

[5] C. C. Wei, K. Z. Chen, L. W. Chen, C. Y. Lin, W. J. Huang, and J. Chen, "High-capacity Carrierless amplitude and phase modulation for WDM long-reach PON featuring high loss budget", IEEE Journal of Lightwave Technology, vol. 35, no. 4, pp. 1075-1082, Feb. 2017.

[6] B. P.S. Sahoo, C. C. Chou, C. W. Weng, and H. Y. Wei, "Enabling Millimeter-Wave 5G Networks for Massive IoT Applications", IEEE Consumer Electronics magazine, vol. 8, pp. 49-54, Jan. 2019.

[7] Z. Zhang, J. Dang, L. Wu, H. Wang, J. Xia, W. Lei, J. Wang, and X. You, "Optical mobile communications: principles, implementation and performance analysis", IEEE Transactions on Vehicular Technology, vol. 68, no. 1, pp. 471-482, Jan. 2019.

[8] J. Son and R. Buyya, "SDCon: integrated control platform for software-defined clouds", IEEE Transactions on Parallel and Distributed Systems, vol. 30, pp. 230-244, Jan. 2017.

[9] D. Soma, Y. Wakayama, S. Beppu, S. Sumita, and T. Tsuritani, "10.16-Peta-B/s dense SDM/WDM transmission over 6-mode 19-core fiber across the C+L band", IEEE Journal of Lightwave Technology, vol. 36, no. 6, pp. 1362-1368, Mar. 2018.

[10] D. Soma, S. Beppu, Y. Wakayama, K. Igarashi, T. Tsuritani, I. Morita, and Masatoshi Suzuki, "257-Tbit/s weakly coupled 10-mode C + L-band WDM transmission", IEEE Journal of Lightwave Technology, vol. 36, no. 6, pp. 1375-1381, Mar. 2018.

[11] M. Nakao, T. Ishihara, and S. Sugiura, "Dual-mode time-domain index modulation for Nyquist-criterion and faster-than-Nyquist single-carrier transmissions", IEEE Access, vol. 5, pp. 27659 -27667, Nov. 2017.

[12] S. Peng, A. Liu, X. Pan, and H. Wang, "Hexagonal multicarrier faster-than Nyquist signaling", IEEE Access, vol. 5, pp. 3332- 3339, Mar. 2017.

[13] M. Chagnon, M. M. Osman, and D. V. Plant, "Half-terabit single-carrier direct-detect transceiver, formats, and DSP: analysis and demonstration", IEEE Journal of Lightwave Technology, vol. 36, no. 2, pp. 447-459, Jan. 2018.

[14] Z. Li, E. Sillekens, L. Galdino, T. Xu, B. C. Thomsen, P. Bayvel, and R. I. Killey, "Digital linearization of direct-detection transceivers for spectrally-efficient 100 Gb/s/λ WDM metro networking", IEEE Journal of Lightwave Technology, vol. 36, no. 1, pp. 27-36, Jan. 2018.

[15] S. T. Le , K. Schuh, M. Chagnon, F. Buchali, R. Dischler, V. Aref, H. Buelow, and K. M. Engenhardt, "1.72-Tb/s virtual-carrier-assisted direct-detection transmission over 200 km", IEEE Journal of Lightwave Technology, vol. 36, no. 6, pp. 1347-1353, Mar. 2018.

[16] K. Zou, Y. Zhu, F. Zhang, and Z. Chen, "200Gbit/s Nyquist 16-QAM half-cycle subcarrier modulation transmission with dual-polarization direct detection", 21st OptoElectronics and Communications Conference/International Conference on Photonics in Switching (OECC/PS), pp. 3-7, Jul. 2016.

[17] J. Tang, J. He, D. Li, M. Chen, and L. Chen,"64/128-QAM half-cycle subcarrier modulation for short-reach optical communications ", IEEE Photonics Technology Letters, vol. 27, no. 3, pp. 284-287, Feb. 2015.

[18] R. Bai, Q. Wang, and Z. Wang, "Asymmetrically clipped absolute value optical OFDM for intensity-modulated direct-detection systems", IEEE Journal of Lightwave Technology, vol. 35, no. 17, pp. 3680-3691, Sep. 2017.

[19] M. Chen, Q. Chen, H. Zhou, Z. Zheng, J. He, and L. Chen, "Low-complexity receiver using under sampling for guard-band SSB-DDO-OFDM", IEEE Photonics Journal vol. 9, no. 4, Article no. 7203012, Aug. 2017.

[20] J. A. Altabas, S. Rommel, R. Puerta, D. Izquierdo, J. I. Garces, and I. T. Monroy, "Nonorthogonal multiple access and carrierless amplitude phase modulation for flexible multiuser provisioning in 5G mobile networks", IEEE Journal of Lightwave Technology, vol. 35, no. 24, pp. 5456-5463, Dec. 2017.

[21] N. Liu, X. Chen, C. Ju, and R. Hui, "40-Gbps vestigial sideband half-cycle Nyquist subcarrier modulation transmission experiment and its comparison with orthogonal frequency division multiplexing", Optical Engineering, vol. 53, no. 9, Article no. 096114, Sept. 2014.

[22] Z. Li, M. S. Erkılınc, K. S. Sillekens, L. Galdino, T. Xu, B. C. Thomsen, P. Bayvel, and R. I. Killey, "Spectrally efficient 168 Gb/s/λ WDM 64-QAM single-sideband Nyquist-subcarrier modulation with Kramers–Kronig direct-detection receivers", IEEE Journal of Lightwave Technology, vol. 36, no. 6, pp. 1340-1346, Mar. 2018.

[23] Y. Zhu, K. Zou, Z. Chen, and F. Zhang,"224 Gb/s optical carrier-assisted Nyquist 16-QAMhalf-cycle single-sideband direct detection transmission over 160 km SSMF", IEEE Journal of Lightwave Technology, vol. 35, no. 9, pp.1557-1565, May 2017.

[24] K. Zhong, X. Hou, Y. Wang, L. Wang, J. Yuan, C. Yu, A. P. T. Lau, and C. Lu, "Experimental demonstration of 608Gbit/s short reach transmission employing half-cycle 16-QAM Nyquist-SCM signal and direct detection with 25Gbps EML", Optics Express, vol. 24, no. 22, pp. 25057-25067, Oct. 2016.

[25] M. M. Ibrahim and R. S. Fyath, "Performance investigation of unamplified C-band Nyquist 16-QAM half-cycle transmission for short-reach optical communications", International Journal of Networks and Communications, vol. 9, no. 1, pp. 1-22, Jan. 2019.

[26] Z. Li, M. S. Erkılınc, K. Shi, E. Sillekens, L. Galdino, T. Xu, B. C. Thomsen, P. Bayvel, and R. I. Killey, "Digital linearization of direct-detection transceivers for spectrally efficient 100 Gb/s/λ WDM metro networking", IEEE Journal of Lightwave Technology, vol. 36, no. 1, pp. 27-36, Jan. 2018.

[27] X. Ruan, K. Li, D. J. Thomson, C. Lacava, F. Meng, I. Demirtzioglou, P. Petropoulos, Y. Zhu, G. T. Reed, and F. Zhang, "Experimental comparison of direct detection Nyquist SSB transmission based on silicon dual-drive and IQ Mach-Zehnder modulators with electrical packaging", Optics Express, vol. 25, no. 16, pp. 19332-19342, Aug. 2017.

[28] K. Zou, Y. Zhu, and F. Zhang, "800 Gb/s (8×100 Gb/s) Nyquist half-cycle single-sideband modulation direct-detection transmission over 320 km SSMF at C-band", IEEE Journal of Lightwave Technology, vol. 35, no. 10, pp. 1900-1905, May 2017.

[29] S. Endo, K. I. A. Sampath, and J. Maeda, "Chromatic dispersion-based modulation distortion compensation for analog radio-over-fiber: performance improvement in OFDM transmission", IEEE Journal of Lightwave Technology, vol. 36, no. 24, pp. 5963-5968, Dec. 2018.

[30] C. Yang, M. Luo, C. Li, W.i Li, and X. Li, "Transmission of 64-Gb/s pilot-assisted PAM-4 signal over 1440-km SSMF with phase noise mitigation", IEEE Photonics Technology, vol. 11, no. 1, Article no. 7200709, Feb. 2019.

[31] S. Chen, C. Xie, and J. Zhang, "Comparison of advanced detection techniques for QPSK signals in super-Nyquist WDM systems", IEEE Photonics Technology Letters, vol. 27, no. 1, pp. 105-108, Jun. 2015.

[32] J. M. Senior, "Optical fiber communications principles and practice", Prentice Hall, Financial Times, England, 2009.

[33] G. P. Agrawal, "Lightwave technology telecommunication systems", Wiley Intersscience, John Wiley, Sons, 111 River Street, Hoboken, NJ 07030, Canada, 2005.

[34] L. N. Binh, "Optical modulation advanced techniques and applications in transmission systems and networks", Taylor and Francis Group, LLC, Boca Raton, London, New York, CRC Press, 2018.